Electromagnetic Non-Destructive Evaluation (XXI)
D. Lesselier and C. Reboud (Eds.)

doi:10.3233/978-1-61499-836-5-33

A Level Set Method for Magnetic Induction Tomography of 3D Boxes and Containers

Oliver DORN [a,1], Alex HILES [a]

[a] *The University of Manchester, UK*

Abstract We present a level set technique for 3D Magnetic Induction Tomography with an emphasis on applications to the screening of small boxes up to cargo containers. A level set method is used for modeling a shape evolution when minimizing a given cost functional. Numerical results will be presented that illustrate the performance of our method in practical situations. A novel line-search technique is introduced that is suitable to control the shape evolution for this computationally demanding MIT inverse problem.

Keywords. Magnetic induction tomography; Shape evolution; Level sets; Nonlinear Kaczmarz; Line search;

1. Introduction

Magnetic Induction Tomography (MIT) has found various applications in the nondestructive testing of materials, see for example [1,4,10] and the references cited there. Recent progress in measurement and detector technology is opening up exciting new applications for this technology, for example in the security screening of small boxes up to cargo containers [6,11]. Mathematically 3D MIT constitutes a highly ill-posed nonlinear inverse problem where appropriate regularization and efficient reconstruction algorithms are essential when facing realistic scenarios. Linearized models have been tested (see for example [10]) but, even though being relatively fast, they quickly reach their limitations regarding resolution and accuracy. Nonlinear schemes seem more promising, even though they still are quite time-consuming and heavy on computer memory consumption. Tailor-made approaches for specific reconstruction, identification and classification tasks are needed for circumventing some of these difficulties. As part of this effort, shape-based techniques for identifying and characterizing hidden objects are developed here that make use of available prior knowledge or assumptions on the materials present in the region of interest. Mathematically this approach has been investigated in [1,7], amongst others. In our contribution we will follow up on this approach and investigate shape based methods for MIT of boxes or containers using a level-set framework [3].

[1] School of Mathematics, The University of Manchester, Oxford Road, Manchester, M13 9PL; E-mail: oliver.dorn@manchester.ac.uk

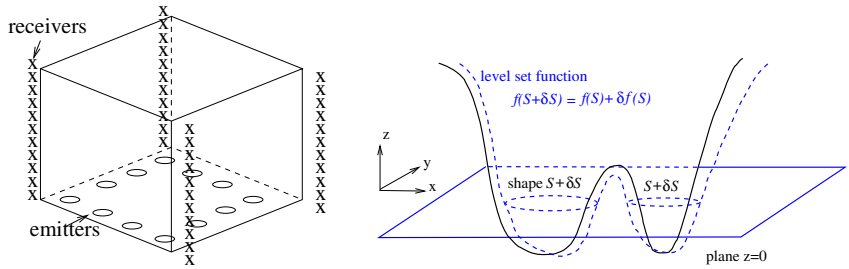

Figure 1. Left: geometric setup of emitters and receivers (here all horizontal coils) around a box-shaped region of interest. Right: cartoon in 2D showing evolution of a level set function for shape propagation.

2. The shape reconstruction problem

2.1. The forward problem

For modelling electromagnetic fields inside the box of interest we use the system of Maxwell's equations in frequency domain

$$\nabla \times \mathbf{E}_j(\mathbf{x}) - a(\mathbf{x})\mathbf{H}_j(\mathbf{x}) = \mathbf{M}_j(\mathbf{x}) \tag{1}$$

$$\nabla \times \mathbf{H}_j(\mathbf{x}) - b(\mathbf{x})\mathbf{E}_j(\mathbf{x}) = \mathbf{J}_j(\mathbf{x}) \tag{2}$$

in a box-shaped domain $\Omega \subset \mathbf{R}^3$, where we imply a time-dependence $e^{-i\omega t}$ for a given frequency $\omega = 2\pi f$. In this study we will assume that the parameter $a(\mathbf{x}) = i\omega\mu(\mathbf{x})$ is known and constant with typical (e.g. free space) values in real and imaginary part. Furthermore, the parameter of interest $b(\mathbf{x}) = \sigma(\mathbf{x}) - i\omega\epsilon(\mathbf{x})$ is 'shape-based' in the sense that it chooses at each location $\mathbf{x}$ in the domain between either an 'internal value' $b_i(\mathbf{x})$ or an 'external value' $b_e(\mathbf{x})$, both being given as known and fixed functions of $\mathbf{x}$. This way $b(\mathbf{x})$ contains discontinuities along closed interfaces $\Gamma \subset \Omega$ that become now the unknowns of our inverse problem. For example, b_i might indicate some 'threat' and b_e some background material of which the specific nature is of no particular interest.

The index j in (1), (2) indicates the different applied source patterns $\mathbf{q}_j = (\mathbf{M}_j, \mathbf{J}_j)^T$, $j = 1, \ldots, p$, for creating the electromagnetic fields. Generalizations of this basic assumption will be addressed in our future research.

In the inverse problem of MIT one is interested in estimating the unknown parameter b from experimentally measured (or simulated noisy) data. In our case, this reduces to the estimation of the interface Γ between internal and external profiles. Practically, we introduce a sufficiently smooth level set function $\phi : \Omega \to \mathbf{R}$ which defines the shape S by

$$b(\mathbf{x}) = \Pi(\phi)(\mathbf{x}) = \begin{cases} b_i(\mathbf{x}) & \text{in} \quad S \quad \text{where } \phi(\mathbf{x}) \le 0, \\ b_e(\mathbf{x}) & \text{in} \quad \Omega \backslash S \quad \text{where } \phi(\mathbf{x}) > 0. \end{cases} \tag{3}$$

The interface $\Gamma = \partial S$ is given by the zero level set $\partial S = \{x \in \Omega : \phi(x) = 0\}$. See the right image of Figure 1 for a visualization of the level set scheme. In our (proof-of-concept style) setup we assume for simplicity that we have p different sources $\mathbf{q}_j$, $j = 1, \ldots, p$, modelled by reasonably sized wire loops or coils (see the left image of Figure 1) located at the bottom of the box or container. Those give rise to the probing fields $\mathbf{E}_j$ and $\mathbf{H}_j$. The

calculated data are $g_j(b) = \mathcal{M}_j \mathbf{E}_j$ where $\mathbf{E}_j$, $\mathbf{H}_j$ solve (1), (2) with parameter b and where $\mathcal{M}_j$ is a (linear) measurement operator which might depend on the source position. In our case, $\mathcal{M}_j \mathbf{E}_j$ are the line integrals of the electric fields along receiving closed wire loops or coils distributed along the four vertical edges of the box (see again Figure 1). We denote the actually measured (or 'true') data by $\tilde{g}_j$. Then, the residuals $\mathcal{R}_j(b)$ and $\mathcal{T}_j(\phi)$ are defined as $\mathcal{R}_j(b) = g_j(b) - \tilde{g}_j$ and $\mathcal{T}_j(\phi) = \mathcal{R}_j(\Pi(\phi))$.

2.2. Gradient calculations by an adjoint scheme

Defining the least squares cost functionals

$$\mathcal{J}_j(b) = \frac{1}{2}\left\|\mathcal{R}_j(b)\right\|_2^2, \quad \text{and} \quad \hat{\mathcal{J}}_j(\phi) = \frac{1}{2}\left\|\mathcal{T}_j(\phi)\right\|_2^2 \tag{4}$$

and the total cost by

$$\mathcal{J}(b) = \sum_{j=1}^{p} \mathcal{J}_j(b) \quad \text{and} \quad \hat{\mathcal{J}}(b) = \sum_{j=1}^{p} \hat{\mathcal{J}}_j(b) \tag{5}$$

we call $\mathbf{grad}_{\mathcal{J}_j,L_2}(b) = \mathcal{R}_j'(b)^* \mathcal{R}_j(b)$ and $\mathbf{grad}_{\hat{\mathcal{J}}_j,L_2}(\phi) = \mathcal{T}_j'(\phi)^* \mathcal{T}_j(\phi)$ the *gradient directions* of expressions in (4) and similar for those in (5). Notice that these gradient directions will depend on the choice of function spaces for the parameter functions b and level set functions ϕ, as indicated in the notation. This will be used when selecting our regularization scheme for the inversion. We have the following *adjoint representation of* $\mathbf{grad}_{\mathcal{J}_j,L_2}(b)$ as shown for example in [2].

Let $\mathbf{E}_j^a$ and $\mathbf{H}_j^a$ be the solution of the following (adjoint) system of Maxwell's equations:

$$\nabla \times \mathbf{E}_j^a(\mathbf{x}) - a(\mathbf{x}) \mathbf{H}_j^a(\mathbf{x}) = 0 \tag{6}$$

$$\nabla \times \mathbf{H}_j^a(\mathbf{x}) - b(\mathbf{x}) \mathbf{E}_j^a(\mathbf{x}) = \mathcal{M}_j^* \overline{\mathcal{R}_j(b)} \tag{7}$$

where $\mathcal{M}_j^*$ denotes the formal adjoint of the measurement operator $\mathcal{M}_j$. Its application amounts to putting the argument (here $\overline{\mathcal{R}_j(b)}$) as artificial 'adjoint sources' at the receiver locations. The overline denotes 'complex conjugate'. Then we have

$$\left[\mathcal{R}_j'(b)^* \mathcal{R}_j(b)\right](\mathbf{x}) = \overline{\mathbf{E}_j(\mathbf{x}) \cdot \mathbf{E}_j^a(\mathbf{x})} \tag{8}$$

where $\mathbf{E}_j$ and $\mathbf{H}_j$ are the solution of (1), (2) with b.

Formal differentiation by the chain rule yields $\mathcal{T}_j'(\phi) = \mathcal{R}_j'(\Pi_j(\phi))\Pi_j'(\phi)$. We have $\Pi_j'(\phi) = (b_i - b_e)\delta(\phi)$. However, the Dirac delta distribution $\delta(\phi)$ will be considered to be approximated by a suitable L_2-function. In our numerical implementations, we will use the narrowband function of thickness d for that purpose. In other words, $\delta(\phi) \approx \chi_{B_d(\Gamma)}$ with $B_d(\Gamma) = \{\mathbf{x} : \text{dist}(\mathbf{x}, \Gamma) \leq d/2\}$ and χ_D denoting the characteristic function of the set D. We have $\mathcal{T}_j'(\phi)^* = \Pi_j'(\phi)^* \mathcal{R}_j'(\Pi(\phi))^*$.

Notice that so far no regularization scheme is applied in order to stabilize the inversion. We will use a regularization scheme explained in more details in [3] which uses suit-

able Sobolev spaces for the gradient calculation (sometimes called 'Sobolev gradients'). This has the effect of replacing the adjoint operator $\mathcal{T}'(\phi)^*$ by a new adjoint operator $\mathcal{T}_j'(\phi)^\circ$ with

$$\mathcal{T}_j'(\phi)^\circ = (\alpha I - \beta\Delta)^{-1}\mathcal{T}_j'(\phi)^*, \qquad \mathbf{grad}_{\hat{\mathcal{J}}_j,W_1}(\phi) = \mathcal{T}_j'(\phi)^\circ\mathcal{T}_j(\phi) \tag{9}$$

and suitably chosen parameters α, β controlling the degree of regularization. The positive definite operator $(\alpha I - \beta\Delta)^{-1}$ has the effect of 'projecting' the gradient $\mathcal{T}_j'(\phi)^*\mathcal{T}_j(\phi)$ from $L_2(\Omega)$ towards a Sobolev space of smoother functions [3].

2.3. A Kaczmarz-type shape reconstruction algorithm

We have presented above gradient directions with respect to the individual cost functionals $\mathcal{J}_j(b)$ which only take into account the part of the complete data set which corresponds to source $\mathbf{q}_j$. The gradient direction which corresponds to the full data set would be a vector whose components are the individual gradient directions $\mathbf{grad}_{\hat{\mathcal{J}}_j,W_1}(\phi)$. However, calculating this combined gradient vector in each step of an iterative reconstruction technique is quite expensive in the case of 3D Maxwell's equations. Therefore, we have adopted in our inversion a single-step ('Kaczmarz-type') reconstruction scheme which follows the general single-step idea of the nonlinear Algebraic Reconstruction Technique (ART) as described in [8]. We perform so-called 'sweeps' over the source positions and only consider the information of one source at a time while calculating an update by an efficient adjoint scheme.

2.4. A novel line search for the Kaczmarz-type shape reconstruction

We have equipped our algorithm with a novel line search strategy which automatically adjusts step sizes at each sweep. First we need to mention that a strict line search as in standard gradient based schemes (using for example a backtracking scheme with a Wolfe or Armijo condition [9]) usually does not work well in a Kaczmarz type algorithm since in each step we are only calculating gradients with respect to one of the p subsets of the data (corresponding to one source position). Searching for a step size that *minimizes* (4) just for the chosen j is not only computationally expensive but also might eradicate some of the progress made when working on the equivalent expressions (4) in previous steps (addressing the other $p-1$ data subsets). A way out is to adopt a step size criterion that guarantees a smooth overall evolution of the shape where each individual update necessarily needs to be sufficiently small in order to preserve previous updates from the other data subsets. In particular, with step sizes chosen to be small, any additional forward solves need to be avoided in the corresponding step size selection process in order not to increase further the already demanding overall computational cost.

Notice that the avoidance of additional forward solves makes it technically difficult to monitor the evolution of (5) accurately. We obtain an *approximation* to (5) by recording values of (4) in each individual step as a by-product of gradient calculation (without adding any forward calculation) and plugging those values into the summation (5) at the end of each sweep. Thereby all forward solves actually contribute to an update, and no forward solve is 'wasted' just for monitoring the evolution of (5). This also means that we do not *enforce* a reduction of the cost (4) (or (5)) in a given step.

Instead, in order to maintain control of convergence of our algorithm, we record the number N_j of voxels that change value (from $b_i(\mathbf{x})$ to $b_e(\mathbf{x})$ or vice versa) in each update. Our aim is to control this number by an inexpensive backtracking line search. Following general ideas of a standard backtracking line search, our goal is to define an interval $I_{target} = [N_{inf}, N_{sup}]$ of values such that $N_j \in I_{target}$ in each update. N_{inf} is chosen to guarantee that sufficient progress is made in each step, and N_{sup} is chosen to make sure that we are not 'overshooting' in the above described sense. We choose the step size γ_j (see the pseudo-code further below) by a traditional backtracking line search, starting with γ_{start} sufficiently large, where however no forward solves are required. For each of the probed γ we neither have to calculate (4) nor (5), but only the corresponding N_j, which is done 'on the fly'.

Implementing this backtracking line search is not difficult, but there remains the question of how to choose γ_{start}. Maybe surprisingly, in our experience the performance of the line search in this particular application of 3D MIT actually depends critically on a clever and dynamic choice of γ_{start} in each sweep! If it is chosen fixed and very large then the backtracking scheme will always stop just below N_{sup}, giving low sensitivity source-sensor pairs the same impact on shape evolution as high-sensitivity pairs. This can lead to a diverging algorithm overall. If it is chosen fixed and small, then the shape evolution might become either extremely slow at certain stages of the algorithm or again (choosing now always values N_j just above N_{inf}) insensitive to the actual sensitivity pattern of the experimental setup.

Therefore we have introduced a dynamic correction of γ_{start} after each sweep, enforcing that the *average* number of voxels $\overline{N} = (\sum_{j=1}^{p} N_j)/p$ that change value per step in each sweep remains inside a smaller interval $[N_{low}, N_{high}]$ with $N_{inf} < N_{low} < N_{high} < N_{sup}$. If $\overline{N} > N_{high}$ in some sweep, γ_{start} is reduced by multiplying it with a value $\tau_1 \in [0.5, 1.0[$. If, on the other hand, $\overline{N} < N_{low}$ in some sweep, then γ_{start} is increased by multiplying it with a value $\tau_2 \in]1.0, 2.0]$. This way we typically obtain a good spread of N_j in each sweep over the entire interval $[N_{inf}, N_{sup}]$ (after a short 'burn-in phase'), making sure that more weight is given to high sensitivity source-receiver pairs (with respect to the current shape boundary) than for low sensitivity source-receiver pairs.

A pseudo-code of the algorithm including the line search is presented in the table.

3. Numerical experiments

We will show two numerical experiments which demonstrate the performance of the general shape-based 3D reconstruction algorithm as well as the novel line search technique proposed in this paper.

The general experimental and computational setup is in both cases the same as displayed in Figure 1. However, the two experiments differ in the dimensions and probing frequency chosen for the screening of the boxes. In Experiment 1 we aim at the screening of small to medium sized boxes where the size of the domain shown in Figure 1 is $2[\mathrm{m}] \times 2[\mathrm{m}] \times 2[\mathrm{m}]$ and the frequency is $f = 10$ MHz. In Experiment 2 we want to screen bigger sized boxes such as cargo containers, where the domain of interest is chosen to be $10[\mathrm{m}] \times 10[\mathrm{m}] \times 10[\mathrm{m}]$ and the frequency is $f = 0.2$ MHz. Notice that the computational domain is actually bigger than the domain of interest shown in Figure 1 since it is surrounded by some outside material (e.g. air). Both, b_e and b_i use constant free space

Algorithm: Single step level set shape reconstruction technique

Initialization:

Specify initial level set function as a signed distance funtion $\phi^{(0)}$;

Choose $[N_{inf}, N_{sup}]$, $[N_{low}, N_{high}]$, γ_{start}, τ_1, τ_2 and put $n = 0$.

Reconstruction:

FOR $m = 1 : M$ (loop over sweeps)

FOR $j = 1 : p$ (loop over source positions)

Calculate $\mathbf{grad}_{\hat{\mathcal{J}}_j, W_1}(\phi^{(n)}) = \mathcal{T}_j'(\phi^{(n)})^{\circ}\mathcal{T}_j(\phi^{(n)})$ by (6)-(9)

Perform backtracking line search for step-size γ_j

Update level set function: $\phi^{(n+1)} = \phi^{(n)} - \gamma_j \mathbf{grad}_{\hat{\mathcal{J}}_j, W_1}(\phi^{(n)})$

Rescale $\phi^{(n+1)} \to \zeta\phi^{(n+1)}$ with scaling parameter $\zeta \in \mathbf{R}^+$.

END

Verify optional stopping criterion.

Adjust, if necessary, γ_{start} *for next sweep.*

END

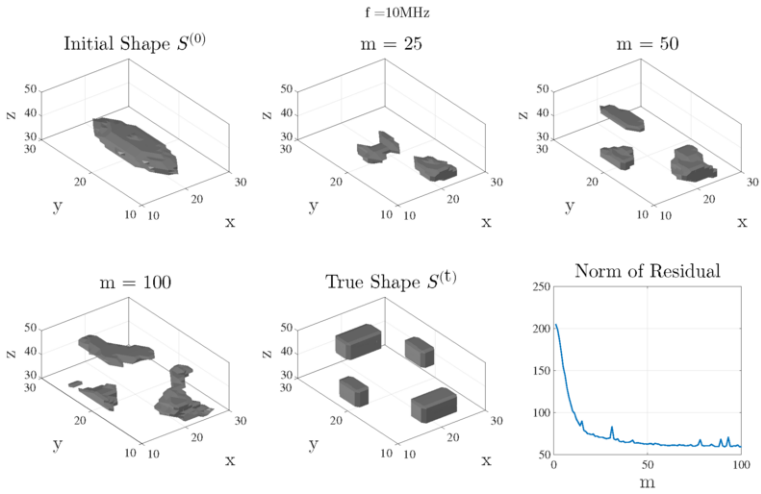

Figure 2. Shape and cost evolution vs sweep number in Numerical Experiment 1 (screening of small to medium sized boxes).

values for ϵ and μ in (1), (2). The conductivity profiles of b_e and b_i inside the box domain are constant with values $0.1\,\mathrm{Sm}^{-1}$ and $0.5\,\mathrm{Sm}^{-1}$, respectively.

In our numerical experiments we are using a finite volume (FV) technique for modelling (1), (2) similar to the one described in [5], but we are also experimenting with an alternative approach using a Finite Differences Frequency Domain (FDFD) technique similar to the one described in [2]. All data are simulated with the same forward model-

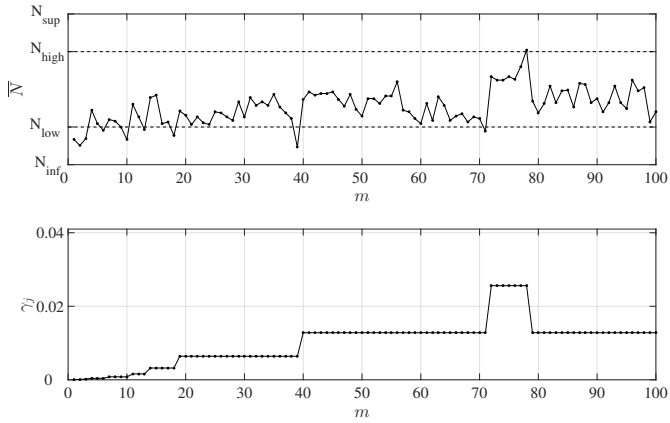

Figure 3. Evolution of $\overline{N}$ (upper image) and γ_j (lower image) vs sweep number in Numerical Experiment 1.

ling code as used in the reconstruction but then 1% Gaussian noise is added to reduce the so-called 'inverse crime'. For the future we plan to generate data with one technique (e.g. FDFD) and do the reconstructions with an alternative technique (e.g. FV).

We have used $[N_{inf}, N_{sup}] = [0, 15]$, $[N_{low}, N_{high}] = [3.75, 11.25]$, $\tau_1 = 0.5$, $\tau_2 = 2.0$ in both numerical experiments. Figure 2 shows the shape evolution and reconstructions of Experiment 1, whereas Figure 4 shows the one of Experiment 2. Figures 3 and 5 show the evolution of the average voxel change per sweep for both experiments, and as a result the evolution of the step size γ_j due to our line search strategy. Both N_{low} and N_{high} are indicated by dashed lines in the upper graph of Figures 3 and 5.

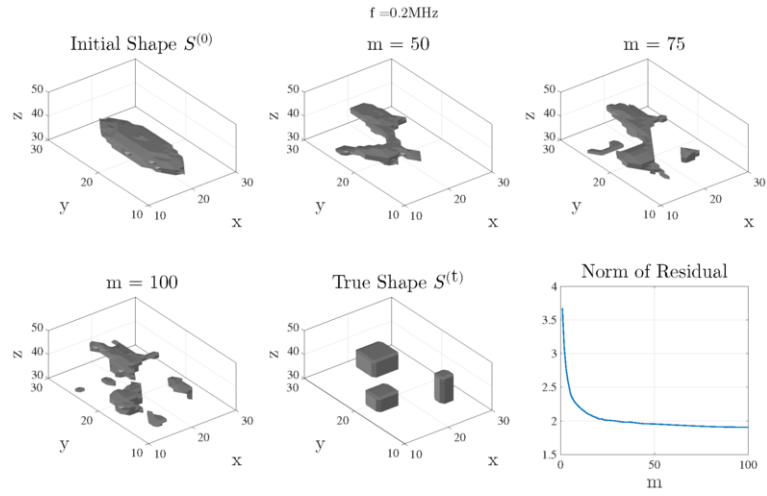

Figure 4. Shape and cost evolution vs sweep number in Numerical Experiment 2 (cargo container screening).

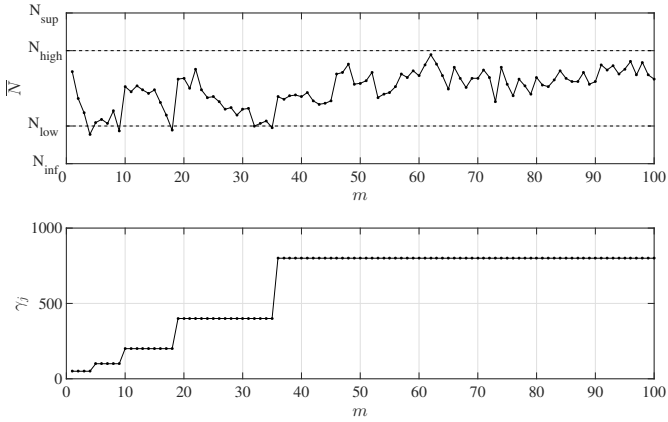

Figure 5. Evolution of $\overline{N}$ (upper image) and γ_j (lower image) vs sweep number in Numerical Experiment 2.

Acknowledgement

The second author acknowledges financial support from the STFC Nuclear Security Science Network.

References

[1] J.F. Abascal, M. Lambert, D. Lesselier, O. Dorn, "3D Eddy-Current Imaging of Metal Tubes by Gradient-Based, Controlled Evolution of Level Sets", *IEEE Trans. Magn.*, **44** (12) 2009.

[2] O. Dorn, H. Bertete-Aguirre, J.G. Berryman and G.C. Papanicolaou, "A nonlinear inversion method for 3D electromagnetic imaging using adjoint fields," *Inverse Problems* No. 15, pp. 1523-1558, 1999.

[3] O. Dorn and D. Lesselier "Level set methods for inverse scattering," Topical Review, *Inverse Problems*, Vol. 22, pp. R67–R131, 2006.

[4] H. Griffiths, "Magnetic induction tomography", *Meas. Sci. Technol.* **12** (2001) 1126–1131.

[5] E. Haber and U. Ascher "Fast finite volume simulation of 3D electromagnetic problems with highly discontinuous coefficients," *SIAM J. Sci. Comput.*, Vol. 6, pp. 1943-1961, 2001.

[6] S. Hussain, L. Marmugi, C. Deans, F. Renzoni, "Electromagnetic imaging with atomic magnetometers: a novel approach to security and surveillance", *SPIE Proc. Vol 9823: Detection and Sensing of Mines, Explosive Objects, and Obscured Targets XXI*, May 2016.

[7] M. Hintermüller, A. Laurain and I. Yousept, "Shape sensitivities for an inverse problem in magnetic induction tomography based on the eddy current model", *Inverse Problems* **31** (2015) 065006.

[8] F. Natterer and F. Wübbeling *Mathematical Methods in Image Reconstruction*, SIAM, Philadelphia, 2001.

[9] J. Nocedal and S. Wright, *Numerical Optimization*, Springer, 1999.

[10] H.Y. Wei and M. Soleimani, "Three-dimensional magnetic induction tomography imaging using a matrix-free Krylov subspace inversion algorithm", *Progress in Electromagnetics Research*, Vol 122, pp 29–45, 2012.

[11] J. Wood, R. Ward, C. Lloyd, P. Tatum, C. Shenton-Taylor, S. Taylor, G. Bagley, M. Joseph and J.C. Watson, "Effect of Shielding Conductivity on Magnetic Induction Tomographic Security Imagery", *IEEE Trans. Magn.* **53** (4) 2017.